ADVANCED ENGINEERING MATERIALS
www.aem-journal.com

Investigation of the Uniformity of Gel Shrinkage by Imaging Tracer Particles Using X-Ray Microtomography

*Anja Hajnal, Mimololorun Lucy Aiyelari, Martin Dirauf, and Pavel Gurikov**

Mass transfer and structural changes in the polymer matrix need to be understood for a rational optimization of the biopolymer-based aerogels production. Herein, the uniformity of changes that occur in the gel structure during the aerogel production by a newly developed method which is based on the imaging of metal tracer particles using X-ray microtomography (X-ray micro-CT) alongside the application of point pattern techniques such as the K-nearest-neighbor (KNN) distances is studied. Agar is initially used as a system of validation for the developed method, after which other polysaccharide and protein-based gels such as alginate, whey protein isolate (WPI), and gelatine are studied. The KNN distance is seen to reduce from hydrogel to aerogel. Furthermore, by means of the KNN distances, the biopolymers are observed to experience a nonuniform distribution of tracer particles correlating to nonuniform shrinkage. Densification at specific sites of the gel represented by lower KNN distance values could be distinguished for each biopolymer. Finally, the spatially resolved polymer network density profile is estimated from the KNN distance by correlating it to experimentally determined polymer network density.

1. Introduction

An aerogel is an open porous, nonfluid/solid colloidal or polymeric network that exhibits low density and high specific surface area.[1–5] Due to the unique combination of physical and chemical properties, aerogels have a wide range of applications in the medical, pharmaceutical, cosmetic, construction, wastewater treatment, environmental pollution, catalysis, and food industries, some of which have been already commercialized and others still in their development phase.[6] According to Brinker and Scherer,[7] the most acceptable viewpoint to classify aerogels is to distinguish them by their composition.[7] In this case, aerogels could be divided into three main categories: inorganic, organic, and inorganic–organic hybrid. The broadest range of various aerogels can be found in the category of inorganic aerogels.[8] From a commercial and scientific perspective, nonpetrochemical feedstock-derived polymers are rapidly gaining ground. Various biopolymers, predominantly polysaccharides and proteins, are used in aerogel production because they are ecological materials that can transform numerous industrial processes from being petroleum dependent into biomaterial dependent. In particular, they have numerous applications in food and nonfood industries.[9,10] However, systematic synthesis of biopolymer-based aerogels only began in the early twenty-first century, and it is still not fully understood how the nature of the polymer, synthesis techniques, and the resulting aerogel structure and properties relates to one another.[1] Fundamental studies into the production of biopolymer-based aerogels will influence the direction of aerogel development in the future.

One of the most critical and much unexplored issues during the production of biopolymer-based aerogels is that of shrinkage.[11,12] The collapse of gel pores during the aerogel processing has a significant impact on the final qualities of the gel. To fully utilize the capabilities of biopolymer aerogels and make it easier to scale up production from a laboratory to a commercial scale, there is still a gap in our knowledge of the shrinkage phenomena that need to be filled. The development of a predictive model that takes into consideration the mass transport phenomena as well as the gel shrinkage during aerogel synthesis is an identified step that would greatly help in the optimization of the production process of biopolymer aerogels. Shrinkage must therefore be investigated more thoroughly in order to do this. Some work has already been done in an attempt to understand the structural changes resulting in shrinkage. One example is the work by Brown et al.[13] in which the effect of different drying methods on shrinkage was studied by implementing X-ray microcomputed tomography, highlighting the power of X-ray microtomography (micro-CT) and its applicability to study the aerogel processing.[13] On its own, however, the resolution of X-ray micro-CT is not high enough to track the changes in

A. Hajnal, M. L. Aiyelari, P. Gurikov
Laboratory for Development and Modelling of Novel Nanoporous Materials
Hamburg University of Technology
Eißendorfer Straße 38, 21073 Hamburg, Germany
E-mail: pavel.gurikov@tuhh.de

M. Dirauf
Institute of Thermal-, Environmental, and Resources' Process Engineering
TU Bergakademie Freiberg
Leipziger Straße 28, 09596 Freiberg, Germany

The ORCID identification number(s) for the author(s) of this article can be found under https://doi.org/10.1002/adem.202301423.

DOI: 10.1002/adem.202301423

the gel during preparation, such as densification at specific sites. As far as we are aware, very little research has been conducted on the gel shrinkage that occurs during the solvent exchange step of aerogel production. These studies also rely on advanced methods that might not be easily or widely accessible. One such study is that by Keidel et al.[14] in which the nonuniform shrinkage of microgels during the solvent exchange was observed using time-resolved small-angle X-ray scattering. It was seen that the gel became denser at its borders and developed a hollow structure in the middle.[14] Another report was given by Dirauf et al.,[15] in which Raman spectroscopy was implemented, and some important insights into the evolution of spatial density distribution of whey protein isolate (WPI) as well as solvent mass transport within the gel matrix were provided.[15]

While the existing studies have shown valuable discoveries in relation to the structural changes that occur during the solvent exchange, they have, however, not taken account of the changes during supercritical drying. In addition, the implemented techniques are not commonly available and can only be applied to the study of a limited range of biopolymer gels. For instance, the biopolymer backbone of typically used diluted gels with a solid mass fraction of 0.5–3 wt% can hardly be analyzed by Raman spectroscopy. Therefore, with the main objective to expand the study on the shrinkage uniformity to a wide range of biopolymers during the complete synthesis of biopolymer-based aerogels in terms of local changes in the spatial density distribution of the gel matrix, we develop a new technique that is nondestructive and broadly applicable regardless of the nature of the gel matrix. The developed method can be broken down into three steps: 1) gelation with entrapment of tracer particles; 2) X-ray micro-CT scanning to detect the tracer particles; and 3) point pattern analysis of micro-CT scans. The fundamental idea behind the novel technique is to prepare gels containing tracer particles and relate the changing position of particles during aerogel processing to changes in the gel structure in terms of shrinkage and densification.

2. Experimental Section

2.1. Materials

Agar–agar granules (ROTH:1347.2) of bioscience grade, ethanol (ROTH: K928.2), silica gel orange (ROTH: P077.2), and dialysis tubing membrane with a flat width of 25 mm ($\varnothing = 16$ mm) and MWCO of 14 000 were purchased from Carl Roth GmbH & Co. KG (Karlsruhe, Germany). Sodium alginate from brown algae powder (Sigma Aldrich: 71 238), gelatine (Sigma Aldrich: 48 723), and D-(+)-gluconic acid δ lactone (Sigma Aldrich: G4750) were purchased from Sigma-Aldrich (Steinheim, Germany). Calcium carbonate (light, precipitated powder, particle size ≈ 10 μm) was provided by Magnesia GmbH (Germany) and carbon dioxide was obtained from Praxair GmbH. WPI (BiPro) was obtained from Davisco Foods International Inc. (Le Suer, MN, USA). Titanium powder with a maximum particle size of 35 μm was used. The water used throughout the study was deionized (pH 6.5–7.0). All reagents were of analytical or food grade and used without further purification.

2.2. Gelation, Solvent Exchange, and Supercritical Drying

Ca–alginate hydrogels were synthesized using the internal setting method.[16] Titanium powder was used as tracer particles and was introduced during the mixing right before gelation. The respective gel mixtures were then poured into disposable 6 mL syringes (internal diameter = 12 mm) and gelled under the required conditions. The gelation of alginate using the internal setting method was fast enough to avoid sedimentation and was carried out exactly according to the above-cited protocol. However, to obtain agar, gelatine, and WPI hydrogel monoliths containing titanium tracer particles, the common protocol using the temperature-induced gelation method needed to be modified.[17] This was because they usually resulted in long gelation times, which led to the sedimentation of particles. To speed up the gelation, agar and gelatine hydrogels were formed by immersing the syringes containing hot biopolymer solutions with tracer particles into an ice bath maintained at 0 °C. WPI hydrogels were obtained by filling the biopolymer solution–tracer mixture into the dialysis tubing membrane and soaking it into hot water, which was preheated to 85 °C and maintained at this temperature. Agar, gelatine, and WPI samples were kept in the corresponding baths for several minutes until the gelation was completed.

To obtain alcogels, the hydrogel cylinders were removed from their respective casings after gelation, and all samples were cut to the required lengths of 12 mm for solvent exchange. In this work, the solvent exchange was carried out by implementing the single-step solvent exchange method as well as the multistep method for different biopolymer gels. For single-step solvent exchange, each cylindrical gel was simply immersed in excess of pure ethanol (150 mL per gel monolith). The ethanol was then changed twice a day for 2 days to ensure a minimum ethanol mass fraction of 98wt% in the pores of the alcogel before drying. For multistep solvent exchange, gels were subjected to ethanol solutions of different concentrations in five steps (150 mL per gel monolith at each step). In each step, the ethanol weight fraction was increased by 20 wt%, and the gels were left in the ethanol–water mixtures for 24 h until equilibrium was established. The solvent exchange was considered completed when ethanol composition reached 98 wt% (all weight fractions were calculated from mixture densities measured with Anton Paar DMA 4500 density meter). After the complete solvent exchange, alcogels were further converted into aerogels by supercritical drying. The description of the supercritical drying equipment can be found in the work by García-González et al.[18] The process of supercritical drying was carried out for a minimum of 3 h at 120 bars and 60 °C to ensure a complete exchange of ethanol present in the pores of the gel with the supercritical CO_2, followed by a 10 min depressurization to ambient pressure.

2.3. X-ray Micro-CT

The SCANCO μCT 35 from SCANCO Medical AG with a resolution of 10 μm was employed in this study. The operating parameters were thoroughly adjusted to not only ensure a good contrast between the tracer particles and the gel background, but also to reduce scanning time because of the possibility of heating

Table 1. X-ray micro-CT parameters for biopolymer gels.

Parameter	Value
Energy/Intensity	70 kVp, 114 μA, 8 W
Voxel Size [μm]	10
Projections/180°	1000
Integration Time [ms]	300
Average Data	2

and shrinkage from prolonged exposure of gels to X-ray beams. **Table 1** sums up important operating parameters.

Usually, the micro-CT scanning requires very little, or no sample preparation and a sample can be scanned exactly as provided. However, because of the rotating sample holder, it was important to load the gels correctly to minimize errors such as the occurrence of artefacts in images due to movement. A sample holder with a diameter of 20 mm and height of 75 mm was used. Because of their light nature, aerogels were mechanically stabilized inside the sample holder with the aid of a sample support, glue, and polystyrene foam. Furthermore, to avoid shrinkage of aerogels while scanning due to humid air, some silica xerogel beads were additionally placed in the sample holder as shown in **Figure 1**.

2.4. Point Pattern Analysis

The K-nearest-neighbor (KNN) algorithm is a widely used supervised machine learning tool in classification or regression problems.[19,20] Additionally, it finds its application in point process statistics, for instance, where the goal is to investigate the geometrical structure of patterns created by randomly dispersed objects in one, two, or three dimensions.[21] The KNN was favored for analyzing the spatial distribution of point patterns partially because of its simplicity, but also due to empirical proof that it was more accurate in predicting a range of data sets compared to other techniques.[21,22] In this context, rather than predicting a class or a continuous value, the KNN was applied to analyze the spatial relationships of particles within a gel. While an alternative algorithm that can be implemented to describe the particle spatial distribution was the radial distribution function, we opted to emphasize the application of the KNN algorithm in this study.[23–26]

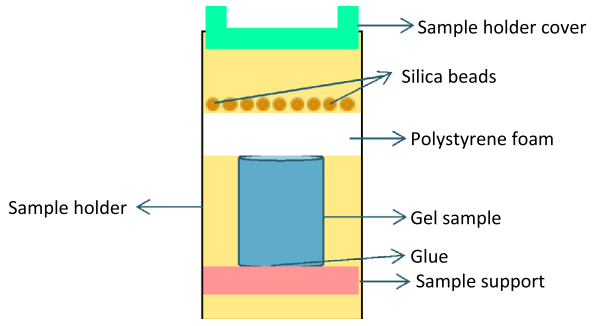

Figure 1. Mounting of (aero)gel sample.

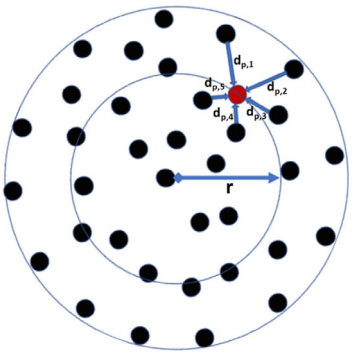

Figure 2. Illustration of KNN implementation. Red particle is the reference particle at the radius r, surrounded by five nearest neighbors.

Tracer particles present in the cross-sectional images were viewed as point patterns dispersed in a finite space of the gel diameter, and the KNN algorithm was implemented in Python for analysis of the changing positions of tracer particles during aerogel synthesis. The illustration of how the KNN distribution was calculated is shown in **Figure 2**.

Using the Euclidean measure, the distance in each horizontal gel cross section between neighboring tracer particles in gels, $d_{\mathrm{p,n}}$, based on the coordinates of the nth neighbour particle $(x_{\mathrm{n}}, y_{\mathrm{n}})$ to some reference particle $(x_{\mathrm{r}}, y_{\mathrm{r}})$ was calculated as follows

$$d_{\mathrm{p,n}} = \sqrt{(x_{\mathrm{r}} - x_{\mathrm{n}})^2 + (y_{\mathrm{r}} - y_{\mathrm{n}})^2} \tag{1}$$

The KNN algorithm can then be implemented to calculate the average neighbor distances for all tracer particles at each radius in the image:

$$\mathrm{KNN}(r) = \frac{\sum_{i=1}^{N_{\mathrm{p}}} \frac{\sum_{n=1}^{K} d_{\mathrm{p,n}}}{K}}{N_{\mathrm{p}}} \tag{2}$$

where K denotes the number of neighbors, $d_{\mathrm{p,n}}$ is the distance between the n-th neighboring particle and the reference particle, and N_{p} denotes the number of particles at the given radius. It is crucial to note that when choosing the value of K, the size of the system being examined and the concentration of tracer particles should always be taken into account. For instance, if a large K value relative to the size of the system is chosen, this would be more computationally expensive and could lead to the loss of information on the local changes. In contrast, if K is too small, more noise is present. Moreover, as the nearest-neighbor distances depend on the particle concentration, it is important to keep this parameter constant between the systems to make them comparable. In this work, the parameter K was set to 5 to help filter some initial noise while still focusing on the immediate neighborhood of each data point to better observe the local changes. Other K values would also be viable options but their effect on the abovementioned aspects and numerical implementation of the algorithm should be carefully assessed.

The KNN was also employed to obtain the local gel network density profile. The gel network density profile used here is defined as the density of the respective gel (hydrogel, alcogel, aerogel) without taking into account the presence of water or ethanol in the pores of

the gel. To compute this so-called "network density" profile from the KNN distributions, the height and diameter at each processing stage as well as the mass of the gel were measured. The aerogel mass was utilized given that the component of an aerogel was only the biopolymer (mass of air was negligible), so the aerogel mass represented the true mass of biopolymer used for production. Relation between the local gel network density and the KNN distribution can be found in the Supporting Information (Section 1).

2.5. Numerical Implementation of KNN on a Random Image

Before analyzing biopolymer gels, an image with a random uniform point distribution to simulate the presence of particles in a gel slice was generated. The image was processed with the developed point analysis method to test and validate the algorithm implementation. Since the particle distribution was random, the average number of particles in a cross-section image, as expected, fluctuated around a mean value that depended on the number of particles within the image cross section or unity when normalized by the average number of particles in the given image cross section, resulting, for a single image (**Figure 3**a), in a noisy KNN distribution (Figure 3b). The magnitude of the deviations from the mean value was an attribute of a sparse and scattered arrangement of particles, which affected the KNN distribution especially at small radii. The "moving average box" smoothing approach was thus used to reduce these noises and allow further application of the distribution for examining the uniformity of shrinkage in gels. The "numpy.convolve" operator in Python was used to perform the moving average box smoothing. It had three modes of operation: full, same, and valid. The data was pulled down at the sides by "full" and "same" smoothing modes due to padding, thereby producing a deceptive depiction of the particle distribution. Therefore, the "valid" mode was implemented because it preserved the data quality at the boundaries and appropriately represented the particle distribution. As the deviations at small radii were larger, the data was mirrored around the gel center to additionally help the smoothening and minimize the edge effects at this boundary. Figure 3 shows a randomly generated image and the KNN distribution obtained before and after smoothing. More information regarding the implementation, as well as the error analysis, can be found in the Section S2 and S6, Supporting Information, respectively.

3. Results and Discussion

3.1. Evolution of Agar Gels during Aerogel Processing

In using agar as a model system for the developed method, two aspects regarding the method standardization were addressed: 1) the selection of an appropriate concentration of titanium tracer particle (TTP) for analysis and 2) the possibility of reinforcement which may lead to reduced shrinkage due to presence of tracer particles inside the gel. From our results, no negative effect of particle mass fraction up to 0.4 wt%TTP on the KNN distribution was noted and neither was any reinforcing effect by the particles on the gels detected. Therefore, 0.2 wt% TTP was chosen as a middle value to work with for further enquiry into the uniformity of shrinkage during aerogel processing. Details about this can be found in Section S3, Supporting Information.

The homogeneity of shrinkage during aerogel processing was studied using agar gels as a model system. **Figure 4**a shows KNN distribution of tracer particles in agar hydrogels, alcogels (obtained by one-step solvent exchange in ethanol), and aerogels normalized by the average KNN distance in the hydrogel cross section. All KNN profiles are an average of 100 profiles (1 mm thickness) in the middle of the corresponding gels. The KNN distance indicates how close the tracer particles are to one another, and it is instructive to see how this distance changes during aerogel production. In Figure 4a, the overall shrinkage of hydrogel when transferred to an aerogel can be observed as indicated by the reduction of the KNN profiles, whereby the linear shrinkage of the gels is proportional to the decrease in the respective KNN values. Another characteristic that is quickly observed in Figure 4a is the high KNN value along the margins of the gels. The maxima were observed for the hydrogel and consistently appeared all the way down to the aerogel. This is due to the initial nonuniform distribution of TTP in agar gels as a consequence of the gelation method. Since the gelation temperature of agar compared to the temperature of dissolution is quite low, a large temperature gradient emerges during the gel formation. This may create in turn a density gradient as the gelation takes place from the edges to the center of the gel, thereby moving particles along this direction.

This observation accentuates that the same piece of gel should ideally be analyzed throughout the aerogel processing, and only

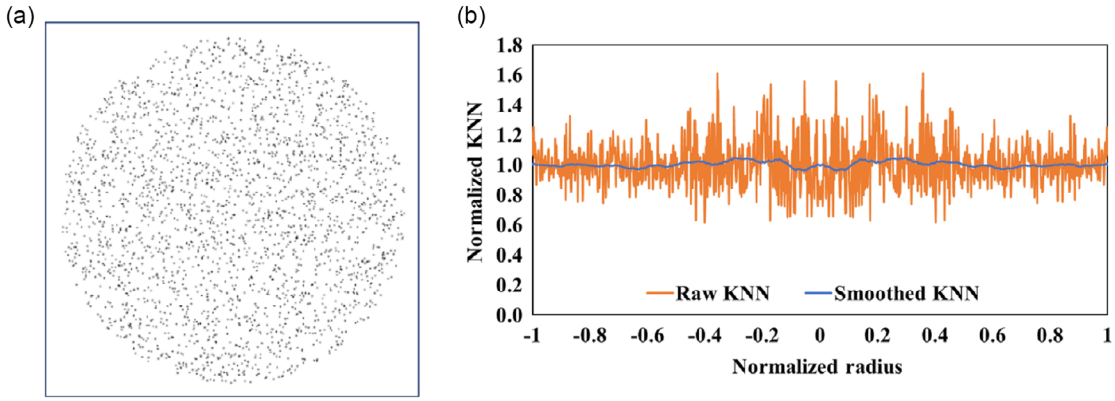

Figure 3. a) Synthetic image with random particle distribution and b) raw and smoothed normalized KNN radial distribution of the randomly generated image.

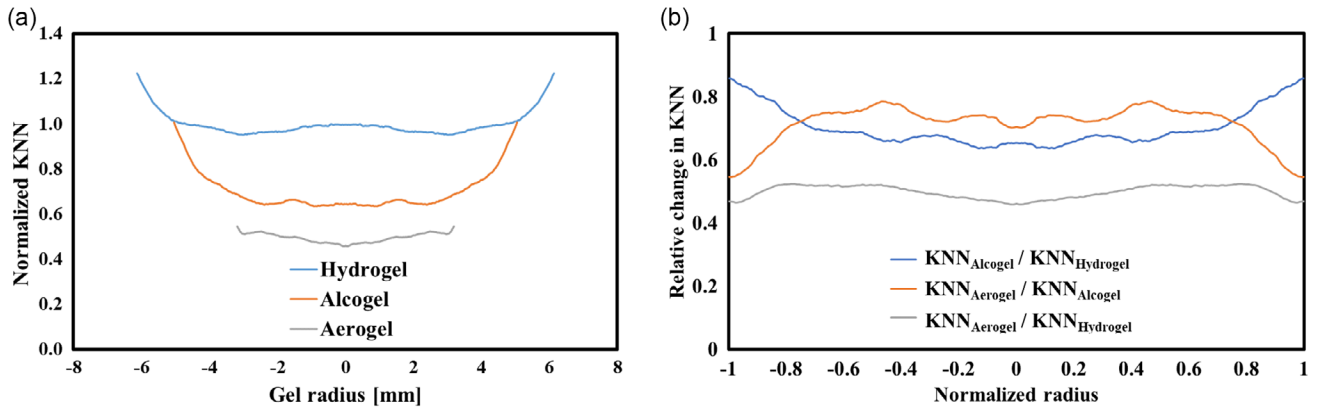

Figure 4. a) Nearest neighbor distribution and b) relative changes in KNN during agar aerogel processing.

relative changes in KNN distributions are informative. Since the initial nonuniform distribution of tracer particles in hydrogels is reflected in the alcogel and aerogel profiles, relative changes in KNN values during solvent exchange (i.e., hydrogel to alcogel), supercritical drying (i.e., alcogel to aerogel), and whole processing (i.e., hydrogel to aerogel) were calculated (Figure 4b).

During the transformation of the hydrogel to alcogel by solvent exchange, the change in the KNN becomes nonuniform, as shown in Figure 4b. The center of the gel decreases in KNN values compared to the edges with a difference of about 20%. This indicates a nonuniform shrinkage during the solvent exchange with densification of biopolymer at the center of the agar gel. This phenomenon of densification at the center during solvent exchange was observed for the first time by Dirauf et al.[15] in their work on the solvent exchange of protein hydrogels and can be explained as a result of the compaction at the center being first affected by mechanical compression from the edges of the gel and then by solvent–polymer interactions afterward.[15] Another possible explanation for densification at the center of the gels during solvent exchange may be an initial densification of the hydrogel at the edges during gelation. Since the edges are denser and mechanically stronger, they have a higher resistance against densification compared to the center of the gels. On analyzing the relative changes in KNN values from alcogel to aerogel during supercritical drying, the opposite can be seen. The KNN values are now lower at the edges relative to the center, implying a nonuniform shrinkage with densification more prominent at the outer parts of the gel. This could be explained by the high-concentration gradients that exist during supercritical drying as well as low compatibility of the polymer with CO_2. The opposing effects of the densification at the center during solvent exchange and at the edges during supercritical drying are both reflected in the matrix distribution of the final aerogel.

Compared to a direct one-step solvent exchange, a multistep solvent exchange significantly reduces shrinkage while better preserving the shape and structure of the gels. This is because adding a step or steps during solvent exchange minimizes concentration gradients that affect the gel.[12] The change in the tracer particle KNN distribution was tracked during a five-step solvent exchange of agar gels in ethanol and observations are shown in **Figure 5**. The average change in KNN during solvent exchange for stepwise

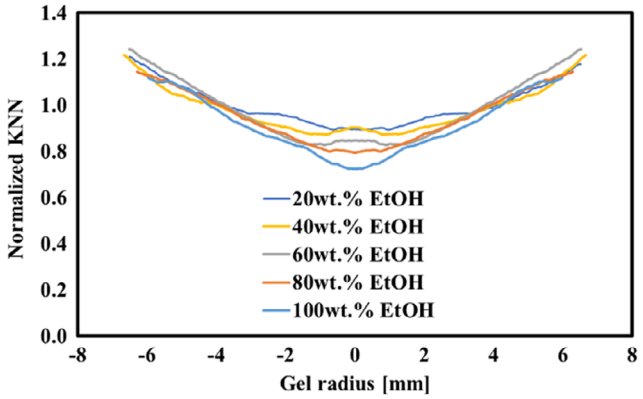

Figure 5. KNN distribution during multistep solvent exchange.

solvent exchange process is less compared to a one-step solvent exchange process. This shows the effect of reducing shrinkage in a multistep solvent exchange process by departing less from equilibrium in the gel system and preventing overstressing of the polymeric network. Furthermore, the overall shrinkage is observed to be mildly nonuniform with a more pronounced effect at the gel center. This observation solidifies the previous observations corresponding to agar and the nonuniform shrinkage during solvent exchange with a densification at the center of the gel. In addition, a very little studied phenomenon in the aerogel processing, namely swelling, was observed between 20 and 40 wt% ethanol. This change of 2% in gel diameter was, however, not large enough to be seen in an increase in KNN profile, due to the error of the used method as discussed in Section S6, Supporting Information. To the best of our knowledge, the swelling phenomenon in the course of the solvent exchange has never been reported in agar gels but known for other systems in the initial steps of the stepwise solvent exchange.[11,27,28]

3.2. Application on Other Biopolymers

In light of the knowledge that biopolymers have different constituents and, as a result, different polymer–solvent interactions which lead to different forms of shrinkage, selected other

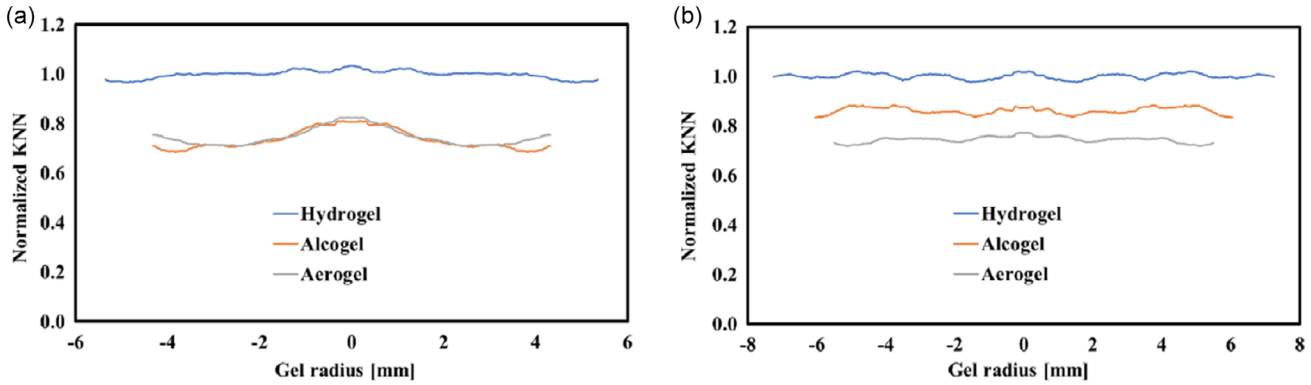

Figure 6. KNN distribution of tracer particles in a) alginate gels and b) WPI gels.

polysaccharide and protein-based biopolymers were observed by analyzing the change in KNN distribution of TTP.

Utilizing crosslinkers, alginate forms gels fast, preventing sedimentation and guaranteeing an initial uniform distribution of tracer particles in the hydrogel. The KNN profiles of tracer particles in alginate gels are shown in **Figure 6**a. A distinctive reduction in average KNN value (27% reduction) from hydrogel to alcogel is observed as the tracer particles are seen to have come closer together after solvent exchange in ethanol, indicating shrinkage. Additionally, the KNN distribution of the alcogel and aerogel are almost identical, implying that supercritical drying of crosslinked alginate gels does not result in significant shrinkage. This is also evident in the equal length of the KNN profiles, which correspond to the gel diameter.

The KNN distribution curves for alginate hydrogel, alcogel, and aerogel show nonuniformity in shrinkage (Figure 6a). While the distribution in the hydrogel is uniform, the same cannot be said for the alcogel and the aerogel. When compared to the center of the gel, the KNN value at the edges of the alcogel is lower by 17%, suggesting that the edges have become denser as a result of solvent exchange. Because ethanol diffuses from the surrounding solvent into the pores of the gel during solvent exchange, the edges of the alginate hydrogel are most affected. It is worthy to note that sometimes during the production of aerogels, some form of nucleation or cavitation can occur which causes the formation of cavities inside the gels. These cavities may not be seen by the naked eye but easily in micro-CT scans (as zones free of tracer particles), and the uniformity can be analyzed using KNN distribution. Some alginate aerogels were observed to contain cavities during preparation. Images of the aerogel alongside the KNN tracer particle distribution are shown in the Section S4, Supporting Information.

The most challenging hydrogels to prepare with tracer particles were WPI hydrogels because WPI forms gels at high temperatures, often in the oven and for a duration of around 60 min, guaranteeing the unwanted total sedimentation of tracer particles before gelation. By preparing WPI hydrogels as described in Section 2.2, tracer particles were successfully dispersed, and the KNN distribution shown in Figure 6b in the hydrogel indicates that this distribution was quite uniform. The decrease in KNN from hydrogel to alcogel further highlights the general gel shrinkage. A noticeable drop in the distribution curve indicates that the particles are closer to one another, and there has been densification of the gel.

Looking closely at the tracer particle KNN distribution curve of the WPI alcogel, a drop is seen at the edges relative to the center of the gel (6% difference). This suggests that as a result of shrinkage, particles gather closer at the borders of the gel than they do in the middle, indicating a form of densification of gels at this site. These changes are actually smaller and less prominent compared to other gels, such as agar, which has a difference between gel border and center values of more than 20%, and alginate, with a difference of about 16%. This may be attributed to the different constituents of biopolymers, which give different levels of densification in ethanol. Furthermore, WPI gels have the highest biopolymer content.

Moreover, in relation to the existing literature on shrinkage uniformity, the densification of WPI seen here correlates with the work done by Dirauf et al.[15] for WPI hydrogels of higher concentration (22.5 wt%).[15] Compared to the center of the 22.5 wt% alcogel, the edges were shown to have a higher protein loading. In the same study, this was, however, not the case for 20 wt% WPI alcogels as a densification of biopolymer was observed at the center of the gel. These contrasting observations at the same WPI concentration (since 20 wt% WPI was also used in this study) may stem from different conditions for hydrogel preparation and sources of WPI, leading to the variations in the gel network structure and constituents leading to different behaviors in the presence of ethanol.

Direct solvent exchange of gelatine gels results in a deformed alcogel with an obviously thicker outer shell than the center. Since it is technically challenging to obtain acceptable scans, this was not used in experiments. Thus, gelatine was subjected to a controlled shrinkage by being first immersed in 70 wt% ethanol and then 100 wt% ethanol, that is, two-step solvent exchange. **Figure 7**a displays the gelatine alcogels prepared by 1) the direct solvent exchange in pure ethanol and 2) two-step solvent exchange. Gelatine alcogels prepared by direct immersion in pure ethanol exhibit a clearly nonuniform shrinkage with polymer compaction around the edges. The vertical lines on the alcogel body indicate the presence of stress on the outer core shell. However, the consistency of shrinkage for gelatine made through a stepwise solvent exchange (Figure 7aii) is not so visually perceptible. In this scenario, the alcogel appears to have been produced stress free and to have shrunk uniformly across its radius.

The KNN distribution during the production of gelatine aerogels created by a two-step solvent exchange in ethanol is depicted

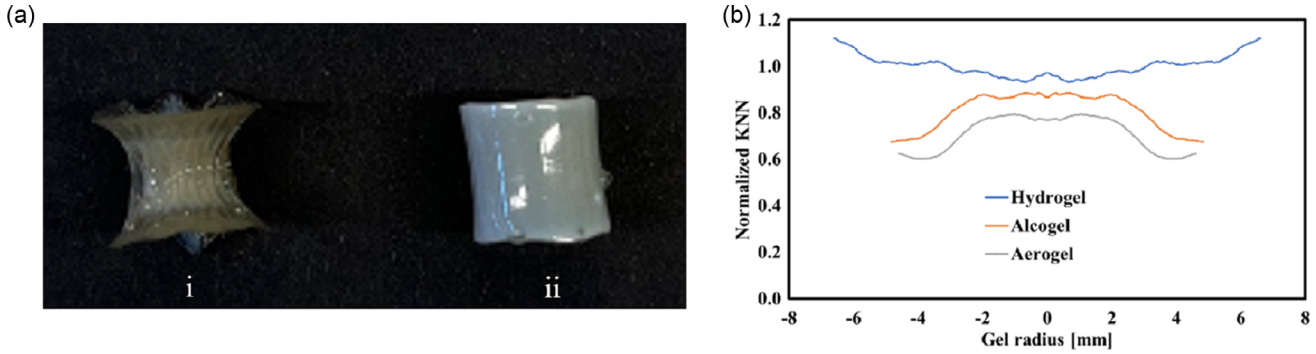

Figure 7. a) Gelatine alcogels obtained by i) direct solvent exchange and ii) two-step solvent exchange and b) KNN distribution of tracer particles in gelatine gels.

in Figure 7b. From hydrogel to alcogel, the nearest-neighbor distances gradually decrease as is typical, indicating shrinkage and overall compaction along the radial direction. However, an interesting phenomenon is seen in the initial change in nearest-neighbor distribution during the production of alcogels. The distribution of nearest-neighbor particles is strongly nonuniform. The alcogel exhibits a downward inversion of this distribution at the edges of the gel in comparison to the hydrogel. This shows that, following solvent exchange, particles are much closer together at the edges of the gel than in the middle. The profiles seen for gelatine as well as other biopolymers, as explained in this section, emphasize even more the value of using tracer particles to examine the homogeneity of shrinkage during the production of biopolymer aerogels.

3.3. Gel Network Density Profile from KNN Distribution

In the pharmaceutical and food industries, the gel network density profile is an important characteristic of the final aerogels produced, as this could have an influence on the drug or flavor release profile. Furthermore, the local changes in porosity could be analogously derived (if the skeletal density is known), which can be useful in mass transfer models. The gel network density profile calculated in this work is defined as the local density of biopolymer without taking into account the presence of water or ethanol in the gel pores, as described in Section S1, Supporting Information. Because the interpore liquid is not considered, there would have been no change in the gel network density if the hydrogel would not shrink during conversion to alcogels and aerogel. The term "gel network density" should not be confused with the gel envelope density.[29] For all biopolymers, the network density profiles were determined from micro-CT images with 1 mm thickness taken in the middle of the gels and given in Section S5, Supporting Information. As a general observation, an overall rise in density consistent with a reduction in KNN distances was noticed.

Additionally, to view the density distribution for the entire vertical gel slice, full-height scans were performed for agar gels processed by the direct one-step solvent exchange in ethanol. A color map of the network density distribution for agar hydro-, alco-, and aerogel is shown in **Figure 8**. The shrinking over the entire height of the gel in terms of biopolymer density can clearly be seen in the color maps. The alcogels produced after the complete solvent exchange, as well as the final aerogel, have a dumbbell shape, as shown in Figure 8b,c. Gel structure, polymer–solvent interactions and the mechanical stress caused by the mass transfer under large solvent concentration gradients are mainly responsible for the occurrence of the shape. It is significant to note that this work made use of agar gels with a weight concentration of 0.5 wt%, although larger weight concentration gels of the same biopolymer type are generally more resistant to shrinkage.[11,15] Furthermore, the change in biopolymer network density from hydrogel to alcogel (Figure 8b), as well as from alcogel to aerogel (Figure 8c), is observed in a change in color from cooler tones to warmer ones showing local shrinkage and network densification.

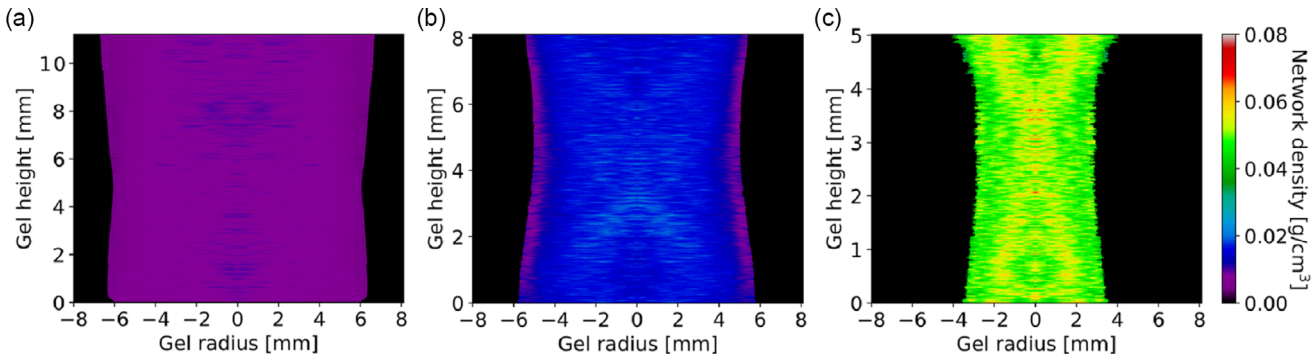

Figure 8. Color maps illustrating network density distribution in agar a) hydrogel b) alcogel, and c) aerogel.

4. Conclusion

In this work, we have developed a novel technique that provides the opportunity to analyze the structural changes that occur during the manufacturing of biopolymer-based aerogels by implementing tracer particles, X-ray microtomography, and point pattern algorithm. Based on the developed technique, we successfully observed the local shrinkage along the gel radii during the production of four different biopolymer-based aerogels by monitoring the KNN distance distribution. The KNN distance was seen to reduce as a result of shrinkage of gels. The nonuniformity of the nearest neighbor distribution was used to demonstrate that all biopolymer types experienced a nonuniform shrinkage. For agar gels, an overall densification toward the center from hydrogel to aerogel was observed. Furthermore, in carrying out a stepwise solvent exchange for agar, the changes in KNN distances were also observed, showing a more moderate and less nonuniform shrinkage as compared to the direct solvent exchange. Alginate, WPI, and gelatine showed opposite behaviors to agar in uniformity of shrinkage. In these cases, the densification was observed to occur toward the gel edges as opposed to the center by a reduction in KNN value. The densification was also seen to be more pronounced in gelatine gels while WPI showed the least prominent densification at the outer parts of the gel. Finally, by correlating the KNN distribution to gel density obtained from experiments, the local radial gel network density distribution was obtained and densification at specific sites in terms of gel network density could be visualized for agar, alginate, WPI, and gelatine gels.

The importance of shrinkage uniformity is linked with key properties of gels and aerogels, which enable their industrial applications (in the pharmaceutical industry for drug loading and release; in advanced food applications for smart ingredient controlling, nutrient release, and delivery systems). The uniformity of shrinkage can now be studied for a variety of biopolymer gels and aerogels. With the developed method, local changes in porosity can also be derived to better understand and model mass transfer processes during biopolymer aerogels production.

Supporting Information

Supporting Information is available from the Wiley Online Library or from the author.

Acknowledgements

The authors gratefully acknowledge support for this research from the German Research Foundation (DFG) under the Project GU 1842/3-1. Furthermore, the authors thank Professor Andreas S. Braeuer (Institute of Thermal-, Environmental, and Resources' Process Engineering, TU Bergakademie Freiberg, Freiberg, Germany) for comments and constructive feedback which helped improve the quality of the manuscript.

Open Access funding enabled and organized by Projekt DEAL.

Conflict of Interest

The authors declare no conflict of interest.

Data Availability Statement

The data that support the findings of this study are available from the corresponding author upon reasonable request.

Keywords

aerogel processing, agar, nearest neighbors, shrinkages, tracer particles

Received: September 6, 2023
Revised: November 7, 2023
Published online:

[1] K. Ganesan, T. Budtova, L. Ratke, P. Gurikov, V. Baudron, I. Preibisch, P. Niemeyer, I. Smirnova, B. Milow, *Materials* **2018**, *11*, 2144.
[2] N. Leventis, A. Sadekar, N. Chandrasekaran, C. Sotiriou-Leventis, *Chem. Mater.* **2010**, *22*, 2790.
[3] F. Liebner, N. Aigner, C. Schimper, A. Potthast, T. Rosenau, *Functional Materials from Renewable Sources*, American Chemical Society **2012**, pp. 57–74, https://doi.org/10.1021/Bk-2012-1107.Ch004.
[4] I. Smirnova, P. Gurikov, *Annu. Rev. Chem. Biomol. Eng.* **2017**, *8*, 307.
[5] D. H. Everett, *Pure Appl. Chem.* **1972**, *31*, 577.
[6] L. E. Nita, A. Ghilan, A. G. Rusu, I. Neamtu, A. P. Chiriac, *Pharmaceutics* **2020**, *12*, 449.
[7] C. J. Brinker, G. W. Scherer, *The Physics and Chemistry of Sol-Gel Processing*, Academic Press **1990**, https://doi.org/10.1016/C2009-0-22386-5.
[8] J. Stergar, U. Maver, *J. Sol-Gel Sci. Technol.* **2016**, *77*, 738.
[9] L. Manzocco, K. S. Mikkonen, C. A. García-González, *Food Struct.* **2021**, *28*, 100188.
[10] S. Zhao, W. J. Malfait, N. Guerrero-Alburquerque, M. M. Koebel, G. Nyström, *Angew. Chem., Int. Ed.* **2018**, *57*, 7580.
[11] P. Gurikov, R. S. P., J. S. Griffin, S. A. Steiner, I. Smirnova, *Ind. Eng. Chem. Res.* **2019**, *58*, 18590.
[12] R. Subrahmanyam, P. Gurikov, P. Dieringer, M. Sun, I. Smirnova, *Gels* **2015**, *1*, 291.
[13] Z. K. Brown, P. J. Fryer, I. T. Norton, R. H. Bridson, *J. Supercrit. Fluids* **2010**, *54*, 89.
[14] R. Keidel, A. Ghavami, D. M. Lugo, G. Lotze, O. Virtanen, P. Beumers, J. S. Pedersen, A. Bardow, R. G. Winkler, W. Richtering, *Sci. Adv.* **2018**, *4*, eaao7086.
[15] M. P. Dirauf, A. Hajnal, P. Gurikov, A. S. Braeuer, *Food Hydrocolloids* **2021**, *120*, 106916.
[16] P. Gurikov, I. Smirnova, *Gels* **2018**, *4*, 14.
[17] P. Harris, *Food Gels* (Ed: P. Harris), Springer, Dordrecht **1990**, https://doi.org/10.1007/978-94-009-0755-3.
[18] C. A. García-González, M. C. Camino-Rey, M. Alnaief, C. Zetzl, I. Smirnova, *J. Supercrit. Fluids* **2012**, *66*, 297.
[19] G. H. Chen, D. Shah, *Found. Trends Mach. Learn.* **2018**, *10*, 337.
[20] O. Kramer, *Dimensionality Reduction with Unsupervised Nearest Neighbors*, Springer Berlin Heidelberg, Berlin, Heidelberg **2013**, https://doi.org/10.1007/978-3-642-38652-7.
[21] J. Illian, A. Penttinen, H. Stoyan, D. Stoyan, *Int. Stat. Rev.* **2008**, *76*, 458.
[22] C. C. Holmes, N. M. Adams, *J. R. Stat. Soc. B* **2002**, *64*, 295.
[23] B. A. F. Kopera, M. Retsch, *Anal. Chem.* **2018**, *90*, 13909.
[24] H. Varela, V!RUS, Sao Carlos **2010**, vol. *3* (accessed: November 2023).

[25] K. Younge, C. Christenson, A. Bohara, J. Crnkovic, P. Saulnier, *Am. J. Phys.* **2004**, *72*, 1247.
[26] X. Zhao, Y. Peng, X. Gang Wang, L. Zhu, H. Chen, *Sci. Rep.* **2019**, *9*, 7885.
[27] S. Boral, A. N. Gupta, H. B. Bohidar, *Int. J. Biol. Macromol.* **2006**, *39*, 240.
[28] C. J. Brinker, G. W. Scherer, *Sol-Gel Science: The Physics and Chemistry of Sol-Gel Processing*, Academic Press **2013**, https://doi.org/10.1016/C2009-0-22386-5.
[29] L. Ratke, P. Gurikov, *The Chemistry and Physics of Aerogels*, Cambridge University Press, Cambridge **2021**, https://doi.org/10.1017/9781108778336.